

SciEn Conference Series: Engineering Vol. 3, 2025, pp 147-152

https://doi.org/10.38032/scse.2025.3.36

# Time-dependent MHD free Convective Heat and Mass Nanofluid Flow through a Vertical Porous Sheet in the Presence of Thermal Radiation

Ashish Barmon and Md Hasanuzzaman\*

Department of Mathematics, Khulna University of Engineering and Technology, Khulna-9203, Bangladesh

# **ABSTRACT**

In the present study, the influences of thermal radiation on time-dependent MHD free convective heat flow and mass nanofluid flow across a vertical permeable sheet have been explored. By applying an effective similarity transformation, the primary partial differential equations (PDEs) are transformed into interconnected nonlinear ordinary differential equations (ODEs). The MATLAB ODE45 tool is used to numerically calculate dimensionless ODEs utilizing the finite difference method (FDM) with shooting technique. Four different water-based nanofluids including copper (Cu), titanium dioxide ( $TiO_2$ ), aluminum oxide ( $TiO_2$ ), and silver (Ag) as a nanoparticles are taken into account. The study explains how non-dimensional parameters such as thermal radiation parameter (R), nanoparticle volume fraction ( $\phi$ ), Prandtl number (Pr), magnetic force parameter (M), and Schmidt number (Sc) affect fluid velocity, temperature, and concentration distribution. The consequences of the volume percentage of copper nanoparticles (up to 4%) on the distributions of velocity, temperature, and concentration are also graphically displayed. The temperature, concentration, and velocity profiles rise with copper nanoparticle volume percentage between 0% and 4%. Increasing volume fraction of nanoparticles ( $\phi$ ) from 0.01 to 0.04 lessen local Nusselt number and boosts skin friction coefficient by 48% and 32%, respectively. As thermal radiation parameter rises from 0.6 to 3.6, skin friction coefficient rises and local Nusselt number drops by 14% and 41%, respectively. Nanofluid Velocity, concentration, and temperature all lessen as the time-dependent parameter's value grows. In conclusion, a comparison was made between our findings and those of the previously published studies. The comparison indicates a high degree of consistency.

Keywords: MHD, nanofluid, thermal radiation.



Copyright @ All authors

This work is licensed under a Creative Commons Attribution 4.0 International License.

## 1. Introduction

Thermal radiation has an impact on the heat and mass transport of nanofluid that travel through a vertical porous sheet. Thermal radiation refers to the term for the transmission of heat utilizing electromagnetic waves, such as infrared radiation. It takes place between the warmed nanofluid and the surroundings. The emissivity of the fluid as well as the temperature difference between the fluid and the surrounding area affect radiative heat transfer. When thermal radiation appears, the topic of study falls under the areas of magneto-hydrodynamics (MHD) and free convection. As it has numerous applications in engineering and industrial processes, this topic is of significant interest in the fields of fluid dynamics, heat transfer, and nanotechnology. Ref. [1] explains how thermal radiation and magnetic fields affect a transitory free circulating nanofluid that is moving toward a vertical plate. Time invariant 2D electro hydro-magnetic boundary layer nano-fluids flow through a porous linear extending plate as the combined impacts of viscous dissipation, Joule heating, and radiative are examined in Ref. [2]. Colloidal suspensions of nanoparticles in an ordinary fluid, such as water or engine oil, are referred to as nanofluid. These nanoparticles enlarge the regular fluid's thermal and mass transfer properties due to their high surface area-to-volume ratio and ability to transfer heat and mass effectively. The presence of nanoparticles in the base fluid alters its thermo-physical properties, making nanofluid highly skilled in various heat exchange

applications, In 1995, Ref. [3] enlarged the idea to nanometer-sized particles and dispersed them within a regular fluid such as water. In Ref. [4], a model was drawn up that took into consideration the effect of nanoparticles' Brownian motion. They also thought this nanofluids' thermal conductivity was separated into two parts. They also computed multiple parameters considering the experimental data for the CuO nanofluid from Ref. [5]. In Ref. [6], a timedependent suction was applied to demonstrate how thermal radiation interacts with an unstable MHD flow via a porous surface. The simultaneous action of thermal radiation and free convection significantly influences the fluid movement and transfer of heat-mass properties in a vertical porous surface when a nanofluid goes under the impact of an external magnetic field (MHD) when temperature variations existent. The Roseland approximation (Ref. [7]), a procedure, is used to explore the radiative heat flux in the energy equation conducted in contrast to research on hybrid systems and traditional nanofluids modified by Al<sub>2</sub>O<sub>3</sub> and Cu with water functioning as the base solvent. Transfer of heat and fluid flow characteristics are all affected by the presence of a magnetic field from outside. The magnetic field generates the Lorentz force, which alters fluid flow patterns and influences the rate of mass and heat transmission. Ref. [8] explored the consequences of chemical reactions and heat radiation on the transient MHD natural convective fluid in the presence of Newtonian heating. Free convection occurs as a result of fluctuations in density brought on by fluid

Published By: SciEn Publishing Group

temperature gradients. immersed in a saturated porous substance. Ref. [9] conducted a study on the analysis of unsteady magnetohydrodynamic convection and mass-heat transport nanofluid flow across an upward perforated sheet. In reference [10], the author examined the impact of diffusion-thermo and thermal dispersion on the uncontrolled transfer of heat and mass in magnetically conducting materials between vertically perforated plates. We expanded upon the work of Ref. [10] in the current investigation by incorporating nanofluids while thermal radiation was present. The influence of the nanofluid on the velocity, concentration, and temperature profiles was investigated. Furthermore, our attention is drawn to how this nanofluid impacts on heat transfer, the coefficients of skin friction, and mass transfer across the edge of the permeable plate. The principal objective of this work is to examine the aforementioned issues by employing a vertically perforated plate and considering the effects of thermal radiation on nanofluid. The main novel contribution of this study lies in the comparison between our numerical results and previously reported findings.

# 2. Model and Governing Equations

The present study considers the analysis of 2D hydromagnetic natural convective boundary layer flow. The flow is assumed to be unstable and includes an electrically conducting and incompressible viscous nanofluid. The flow occurs over a vertical permeable sheet that is embedded in a porous medium. The positioning of the plate occurs along the x-axis. The orientation of the vertical porous plate is aligned parallel to the direction of the free-stream velocity. The yaxis is oriented at a right angle to the vertical porous sheet. A transverse uniform magnetic field with a strength of  $B_0$  is applied to the flow. The temperature and concentration of the fluid at the wall are denoted as  $T_w$  and  $C_w$ , respectively. For t > 0, the porous plate commences the process of transferring fluid through its surface with a velocity denoted as U. Figure 1 exhibits the arrangement of the flow and coordinate system. The velocity of the fluid is only dependent on the variables of time (t) and position (y). Applying the Boussinesq approximation, the fluid is governed by the following equations represented by Ref. [10]

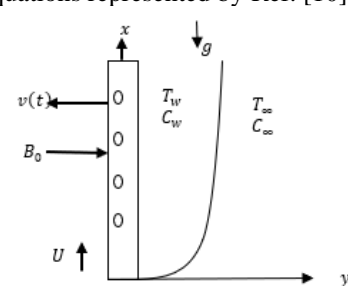


Figure 1: Coordinates system and physical model

$$\frac{\partial u}{\partial t} + v \frac{\partial u}{\partial y} = v_{nf} \frac{\partial^2 u}{\partial y^2} + g \beta_{nf} (T - T_{\infty})$$

$$+ g \beta_{nf}^* (C - C_{\infty}) - \frac{\sigma'_{nf} B_0^2 u}{\rho_{nf}}$$

$$\frac{\partial T}{\partial t} + v \frac{\partial T}{\partial y} = \alpha_{nf} \frac{\partial^2 T}{\partial y^2} + \frac{D_{mnf} k_T}{C_s C_p} \frac{\partial^2 C}{\partial y^2} - \frac{1}{(\rho C_p)_{nf}} \frac{\partial q_r}{\partial y}$$

$$\frac{\partial C}{\partial t} + v \frac{\partial C}{\partial y} = D_{mnf} \frac{\partial^2 C}{\partial y^2} + \frac{D_{mnf} k_T}{T_m} \frac{\partial^2 T}{\partial y^2}$$
The boundary conditions relevant to this issue are

$$+g\beta_{nf}^{*}(C-C_{\infty}) - \frac{\sigma_{nf}'B_{0}^{2}u}{\rho_{nf}}$$
 (2)

(1)

$$\frac{\partial T}{\partial t} + v \frac{\partial T}{\partial y} = \alpha_{nf} \frac{\partial^2 T}{\partial y^2} + \frac{D_{mnf} k_T}{C_S C_p} \frac{\partial^2 C}{\partial y^2} - \frac{1}{(\rho c_p)_{nf}} \frac{\partial q_r}{\partial y}$$
(3)

$$\frac{\partial C}{\partial t} + v \frac{\partial C}{\partial y} = D_{mnf} \frac{\partial^2 C}{\partial y^2} + \frac{D_{mnf}k_T}{T_m} \frac{\partial^2 T}{\partial y^2}$$
 (4)

The boundary conditions relevant to this issue are

$$= U(t), v = v(t), T = T_w, C = C_w \text{ at } y = 0$$
 (5)

$$u = U(t), v = v(t), T = T_w, C = C_w \text{ at } y = 0$$
 (5)  
 $u = 0, v = 0, T \to T_{\infty}, C \to C_{\infty} \text{ at } y \to \infty$  (6)

where (u, v) denotes nanofluid velocity components of in the x - and y - directions respectively. T,  $T_w$ , and  $T_\infty$ denote nanofluid the temperature, wall temperature, and free stream temperature respectively. The acceleration owing to gravity is denoted by the symbol  $g. C_s, C$ , and  $C_{\infty}$  denote the nanofluid concentration susceptibility, concentration, and concentration in the free stream respectively.  $T_m$  and  $k_T$ denote the nanofluid mean temperature and thermal diffusion ratio respectively. The symbol  $D_{m_{nf}}$  denotes the coefficient of mass diffusivity.  $\rho_{nf}$ ,  $\mu_{nf}$ ,  $k_{nf}$ ,  $(\rho c_p)_{nf}$ ,  $\beta_{nf}$ , and  $\sigma'_{nf}$ denote nanofluid the density, dynamic viscosity, thermal conductivity, heat capacity at constant pressure, volumetric expansion coefficient, and electrical respectively which are defined by Ref. [11, 12].

$$\alpha_{nf} = \frac{k_{nf}}{(\rho c_p)_{nf}}, \mu_{nf} = \frac{\mu_f}{(1 - \varphi)^{2.5}}, \beta_{nf} = (1 - \varphi) \beta_f + \varphi \beta_s, \ (\rho c_p)_{nf} = \varphi(\rho c_p)_s + (1 - \varphi) (\rho c_p)_f,$$

$$\begin{split} \rho_{nf} &= (1 - \varphi) \rho_f + \varphi \rho_s, \frac{k_{nf}}{k_f} = \\ &\frac{(2k_f + k_s) - 2\varphi(k_f - k_s)}{(2k_f + k_s) + \varphi(k_f - k_s)}, \, \beta_{nf}^* = (1 - \varphi) \, \beta_f^* + \varphi \beta_s^* \end{split}$$

In the given equation, the symbol  $\varphi$  represents the volume fraction of nanoparticles in the system. A value of  $\varphi = 0$ signifies the absence of nanoparticles, indicating a base fluid. The variables  $\rho_s$  and  $\rho_f$  represent the densities of thenanoparticles and ordinary fluid respectively. Similarly,  $\beta_s$  and  $\beta_f$  indicate the volumetric expansion coefficient of nanoparticles and ordinary fluid respectively. The variables  $k_s$  and  $k_f$  indicate the thermal conductivities of the nanoparticles and ordinary base fluid respectively. Additionally, $(\rho c_p)_s$  and  $(\rho c_p)_f$  indicate the heat capacitance of the nanoparticles and ordinary fluid respectively. Lastly,  $\sigma_s'$  and  $\sigma_f'$  denote the electrical conductivities of the nanoparticles and ordinary fluid respectively. By a similarity parameter  $\sigma$  as

$$\sigma = \sigma(t) \tag{7}$$

The solution to equation (1) is represented in relation to the time-varying magnitude  $\sigma$  in the following manner:

$$v = -v_0 \frac{v}{\sigma} \tag{8}$$

where the time-dependent length scale is  $\sigma$ . The velocity of the sheet, which does not have any units, is represented by the symbol  $v_0$ . If the initial velocity  $v_0$  is negative, it shows the existence of wind blowing. On the other hand, if  $v_0$  is a positive value, it indicates the presence of suction.

The radiative heat flow $(q_r)$  is provided in Ref. [13]

$$q_r = -\frac{4\sigma^*}{3K^*} \frac{\partial T^4}{\partial y} \tag{9}$$

The symbol  $\sigma^*$  indicates the Stefan-Boltzmann constant, whereas  $K^*$  represents the mean absorption coefficient. According to the stated reference (Ref. [14]), it is hypothesized that the temperature changes inside the flow are insignificant. This allows for the simplification of a linear correlation between temperature measurements. By using a Taylor series expansion centered at  $T_{\infty}$  and neglecting higher-order variables, the approximation of  $T^4$  may be approximated as roughly equal to  $4T_{\infty}^3T - 3T_{\infty}^4$ .

We propose the following similarity transformation to

simplify the mathematical study of the problem Ref.[10] 
$$\theta(\eta) = \frac{T - T_{\infty}}{T_{W} - T_{\infty}}, \eta = \frac{y}{\sigma}, \phi(\eta) = \frac{C - C_{\infty}}{C_{W} - C_{\infty}}, f(\eta) = \frac{u}{U}$$
 (10)

The equations (1)-(4) are converted into dimensionless coupled ordinary differential equations (ODEs) using the

equations as mentioned above (7)-(10): 
$$f''(\eta) + \frac{(1-\varphi)^{2.5}\{(1-\varphi)\rho_f + \varphi\rho_s\}\{(1-\varphi)\beta_f + \varphi\beta_s\}}{\rho_f\beta_f} Gr \ \theta(\eta) + \frac{(1-\varphi)^{2.5}\{(1-\varphi)\rho_f + \varphi\rho_s\}\{(1-\varphi)\beta_f^* + \varphi\beta_s^*\}}{\rho_f\beta_f^*} Gm \ \varphi(\eta) - \frac{(1-\varphi)^{2.5}\{(1-\varphi)\rho_f + \varphi\rho_s\}}{\sigma_f'} Mf(\eta) = \frac{(1-\varphi)^{2.5}\{(1-\varphi)\rho_f + \varphi\rho_s\}}{\rho_f} \xi f'(\eta)$$

$$\frac{(1+R\frac{k_f}{k_nf})}{\rho_f} \theta''(\eta) + \frac{\alpha_f\{(k_s+2k_f)-2\varphi(k_f-k_s)\}(\rho c_p)_f}{\{(1-\varphi)\alpha_f + \varphi\alpha_s\}\{(k_s+2k_f)+\varphi(k_f-k_s)\}\{(1-\varphi)(\rho c_p)_f + \varphi(\rho c_p)_s\}} Df \phi''(\eta) = -2\frac{\alpha_f}{\{(1-\varphi)\alpha_f + \varphi\alpha_s\}} \xi \theta'(\eta)$$
(12)
$$\frac{1}{sc} \phi''(\eta) + Sr\theta''(\eta) = -2\frac{\{(k_s+2k_f)+\varphi(k_f-k_s)\}\{(1-\varphi)(\rho c_p)_f + \varphi(\rho c_p)_s\}}{\{(k_s+2k_f)-2\varphi(k_f-k_s)\}(\rho c_p)_f} \xi \phi'(\eta)$$
(13)
The converted boundary conditions are provided by  $f = 1, \ \theta = 1, \ \phi = 1 \ when \ \eta = 0$ 
(14)
$$f = 0, \ \theta = 0, \ \phi = 0 \ when \ \eta \to \infty$$

where 
$$Gr = \frac{g\beta_f(T_W - T_\infty)\sigma^2}{Uv_f} = \text{local Grashof number}, \ Pr = \frac{v_f(\rho c_p)_f}{k_f} = \text{Prandtl number}, \ M = \frac{\sigma_f' B_0^2 \sigma^2}{\rho_f v_f} = \text{magnetic force}$$
 parameter,  $Df = \frac{D_{mf}k_T(C_W - C_\infty)}{C_S C_p v_f(T_W - T_\infty)} = \text{Dufour number}, \ Gm = \frac{g\beta_f^*(C_W - C_\infty)\sigma^2}{Uv_f} = \text{modified local Grashof number}, \ Sr = \frac{D_{mf}k_T(T_W - T_\infty)}{v_f T_m(C_W - T_\infty)} = \text{Soret number}, \ Sc = \frac{v_f}{D_{mf}} = \text{Schmidt number}, \ R = \frac{16\sigma^*T_\infty^3}{3k^*k} = \text{Radiation number}, \ \text{and} \ \xi = \eta + \frac{v_0}{2} = \text{time}$  dependent parameters

# 3. Flow parameters

The Nusselt number, the Sherwood number, and the skin friction coefficient are the flow parameters defined in the following way:

following way:  

$$Nu = -\frac{k_{nf}}{k_f} \theta'(0), Sh = -\frac{D_{mnf}}{D_{mf}} \phi'(0), and$$

$$Cf = \frac{1}{(1-\varphi)^{2.5}} \frac{1}{Re_x} f'(0)$$
(16)

# 4. Results and Discussion

This computational work evaluated unstable MHD convection and transport of heat-mass of nanofluid flow across an upright permeable sheet under thermal radiation. The FDM with shooting approach in MATLAB ODE45 is used to numerically solve the ODEs (10)–(12). Mathematical have been formulated for temperature, concentration, and velocity, utilizing different estimations of appropriate non-dimensional flow parameters, to determine the physical significance of the situation. Volume fraction  $(\varphi)$  measurements of nanoparticles are taken within the range of 0.0 to 0.04. The common fluid Prandtl number (Pr) remains constant at a value of 6.8. When  $\varphi = 0$ , the model prioritizes the analysis of the macroscopic properties and

behavior of a viscous fluid, disregarding the nanoscale features. Figures 2-10 visually demonstrate the influence of appropriate dimensionless flow parameters on the velocity, temperature, and temperature distribution of the Cu-water nanofluid are illustrated graphically in Figures 2-10. The numerical amounts of  $(-\theta'(0))$ , (f'(0)), and  $(-\phi'(0))$  for various parameters are provided in Tables 1-2. Figure 2 demonstrates how the heat radiation parameter (R) affects the velocity pattern. The heat radiation parameter's value may be determined by utilizing the formula  $R = \frac{16\sigma^* T_{\infty}^3}{3k^*k}$  and shapes in the enhanced thermal diffusion term in Eqn. (12)

i.e.  $\frac{(1+R\frac{k_f}{k_nf})}{p_r}\theta''(\eta)$ . The heat radiation parameters identify the relative importance of thermal radiation to thermally conductive transfer of heat. Thermal radiation gets dominance over thermal conduction when R>1, but thermal conduction gets dominance when R<1. When R=1, heat radiation and thermal conduction both contribute equally. For the current simulations, we confine our attention to the scenario when R>1. The linear velocity grows strongly as Rincreases, as illustrated in Figure 2. If the flow is strengthened, the expansion of temperature improves and the expansion of velocity drops. The thickness of the boundary layer diminishes as a consequence of this momentum. How the heat radiation parameter (R) influences the temperature profile is demonstrated in Figure 3. As the value of the thermal radiation parameters rises, the surface temperature gradient diminishes, depicted in Figure 3. On the surface, as R grows, the heat transmission rate reduces. The thickening of the thermal border is prompted by the thermal radiation. The system cools because heat energy is lost by the fluid movement in the flow zone.

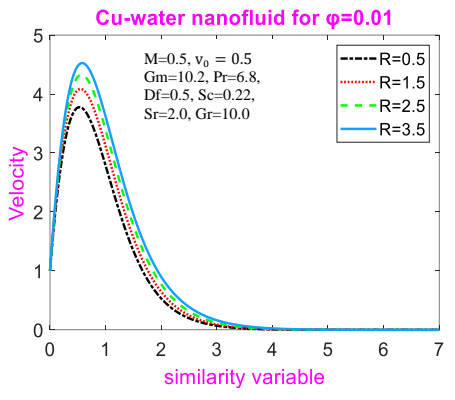
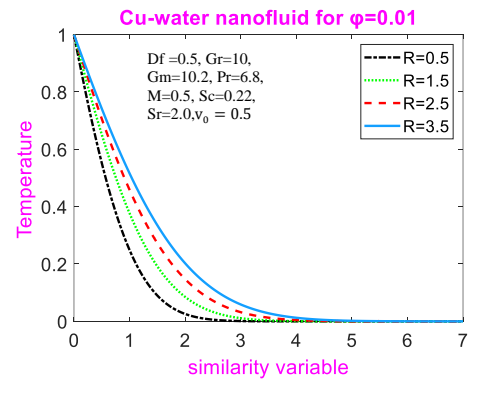


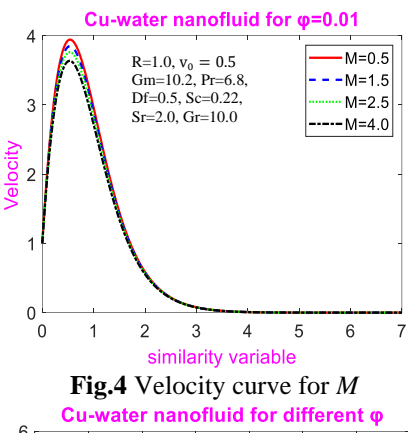
Fig.2 Velocity curve for R



**Fig.3** Temperature curve for *R* 

For a variety of magnetic force parameter (M) values, the velocity distribution is exhibited in Figure 4. As the magnetic

force parameter goes up, Figure 4 depicts how the fluid velocity drops. A resistive force, such as a pulled force, develops as the magnetic force parameter value rises. Lorentz force is a term utilized to refer to this resistive force type. The fluid's motion is slowed down by this Lorentz force, which hinders it. That is, as M values go up, the velocity distribution gets lower. In Figure 5, the velocity curve is altered by the copper nanoparticles volume percentage. An ordinary fluid's characteristics may be greatly enhanced by adding nanoparticles, which may boost heat transfer, thermal conductivity, and even mechanical performance. The velocity profile develops when we take nanofluid into thought rather than base fluid.



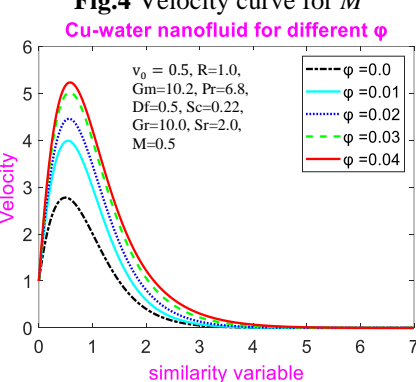


**Fig.5** Velocity curve for  $\varphi$ 

With an increase in the volume percentage of the nanoparticle between 0.0 and 0.04, the boundary layer velocity profile grows stronger. The impact of the copper nanoparticle volume fraction  $(\varphi)$  on the temperature distribution is apparent in Figure 6. Boosting the estimate of  $(\varphi)$  boosts temperature distribution by improving the nanofluid's thermal conductivity. The temperature and velocity profiles of various types of nanofluids containing Ag, Cu,  $Al_2O_3$ , and  $TiO_2$  as nanoparticles, with a nanoparticle volume fraction  $(\varphi=1\%)$ , are illustrated in Figures 7 and 8.

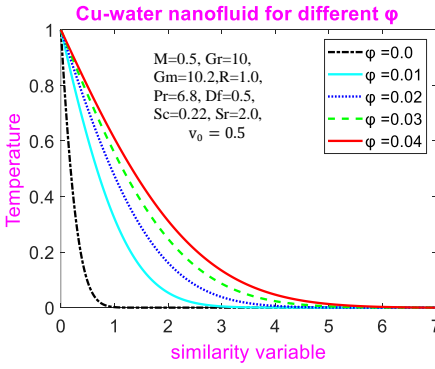


**Fig.6** Temperature curve for  $\varphi$ 

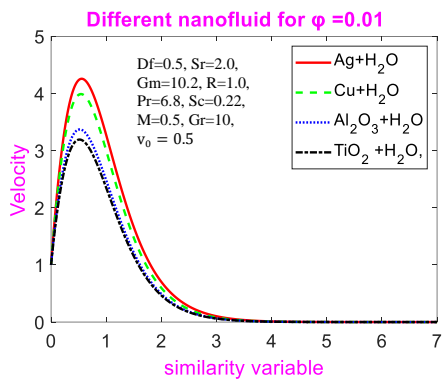


Fig.7 Velocity curve for different nanofluid

As shown in Figure 7, the velocity profile increases as one transitions from  $TiO_2$  to Ag. Among other reasons, Ag possesses a high thermal conductivity. A greater thermal conductivity can diminish frictional force. Thus, particles of fluid can readily flow. As temperature increases, the profile changes from  $TiO_2$  to Ag. Various variations of the Schmidt number (Sc) are utilized to display the velocity curve in Figure 9. Schmidt number (Sc) and kinematic viscosity are intimately related. The fluid viscosity increases as Sc advances, therefore slowing down the fluid flow. Due to this factor, the fluid particles have limited mobility. Thus, the fluid's velocity falls. When Sc goes up, the thickness of the momentum border layer goes down.

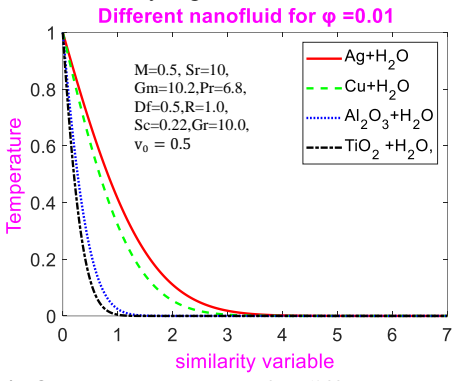


Fig.8 Temperature curve for different nanofluid

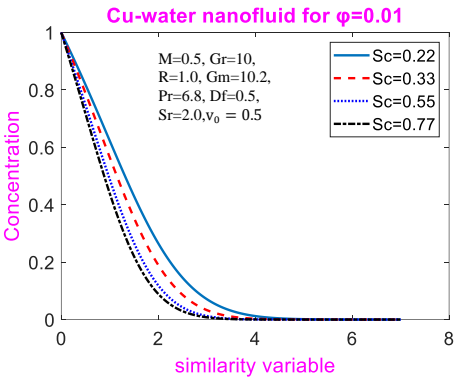


Fig.9 Concentration curve for Sc

Figure 10 illustrates how the temperature distributions are greatly affected by the Prandtl number (Pr). The non-dimensional Prandtl number is represented by the ratio of dynamic viscosity to heat conductivity. The fluid's viscosity rises with a rise in the Prandtl number, which causes the fluid's flow velocity to drop. The fluid particles are unable to flow freely as a consequence. As Pr grows, the fluid's

velocity consequently drops. Figure 11 represents the variations in velocity profile that occur as an outcome of the time-dependent parameter ( $\xi$ ) being utilized. Nanofluid velocity lessens as the time-dependent parameter's value advances.

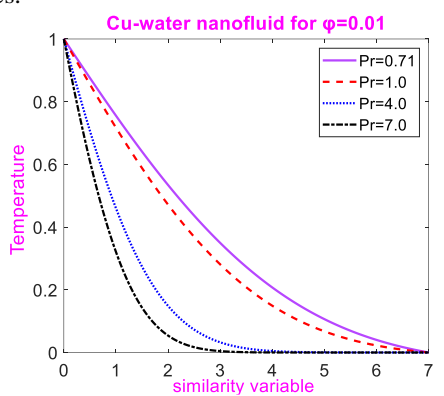
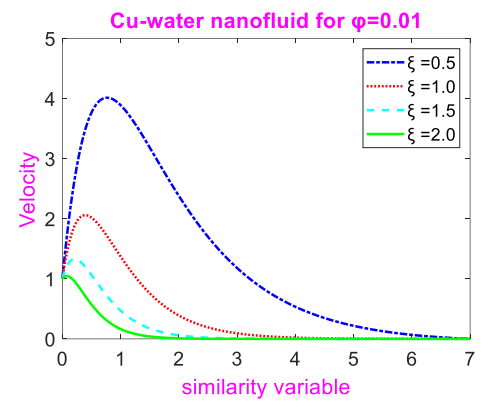


Fig.10 Temperature curve for Pr



**Fig.11** Velocity curve for  $\xi$ 

Table 1. Values of  $(-\theta'(0))$ , (f'(0)), and  $(-\phi'(0))$  for different R

different K				
R	f'(0)	$(-\theta'(0))$	$(-\phi'(0))$	
0.6	13.1137939	68.514393× 10 <sup>-2</sup>	0.605060	
1.6	13.9109416	53.656235× 10 <sup>-2</sup>	0.605060	
2.6	14.5103929	45.736868× 10 <sup>-2</sup>	0.605060	
3.6	14.9959357	40.625642× 10 <sup>-2</sup>	0.605060	

Table 1 displays the impact of thermal radiation (R) on  $(-\theta'(0)), (f'(0))$ , and  $(-\phi'(0))$ . Table 1 demonstrates a decline in the rate of heat transfer, while the coefficient of local skin-friction increases with higher levels of R. As the values of R increase from 0.6 to 3.6, the value of  $(-\theta'(0))$  lessens by about 41%, and f'(0) increases by approximately 14%. That's why, as shown in Figures 2 and 3, the fluid's speed and temperature go up as R goes up.

Table 2. Values of  $(f'(0)), (-\phi'(0))$ , and  $(-\theta'(0))$  for different  $\varphi$ 

φ	f'(0)	$(-\theta'(0))$	$(-\phi'(0))$
1%	13.113793	0.6851439	0.6050601
2%	14.597042	0.4952285	0.5943722
3%	16.602942	0.4092544	0.5839787
4%	17.395849	0.3575089	0.5738605

The values of  $(-\phi'(0))$ ,  $(-\theta'(0))$ , and (f'(0)) are displayed in Table 2 indicating distinct values of the copper nanoparticle volume fraction  $(\varphi)$ . Table 2 reveals that as  $\varphi$  increases, the numerical values of f'(0) boost while the numerical values of  $(-\theta'(0))$  and  $(-\phi'(0))$  fall. Furthermore, the value of f'(0) experiences a 32% increase, whereas the values of  $(-\theta'(0))$  and  $(-\phi'(0))$  drop by 48% and 5%, respectively, as a consequence of the increase in  $\varphi$  values from 0.01 to 0.04. When the value of  $\varphi$  is increased, there is a corresponding rise in concentration, velocity, and temperature respectively.

# 5. Conclusions

This work examined a numerical observation of the timesensitive MHD free convection and heat-mass transport of the nanofluid via a perforated sheet in the presence of heat radiation. It is possible to draw the following conclusions from the numerical models:

- A larger value of R causes the nanofluid' temperature and velocity to go up.
- The nanofluid velocity, concentration, and temperature accelerate due to improving of the the nanoparticles volume fraction of copper.
- A greater Prandtl number results in a decline in the velocity of the nanofluid.
- The nanofluid velocity and temperature profiles advances from  $TiO_2$  to Ag.
- Reduced velocity of the nanofluid follows from greater amounts of *M*.

#### References

- [1] M.A. Kumar, Y.D. Reddy, V.S. Rao, B.S. Goud, Thermal radiation impact on MHD heat transfer natural convective nanofluid flow over an impulsively started vertical plate, Case Stud. Therm. Eng. 24 (2021), 100826.
- [2] Y.S. Daniel, Z.A. Aziz, Z. Ismail, F. Salah, Effects of thermal radiation, viscous and Joule heating on electrical MHD nanofluid with double stratification, Chin. J. Phys. 55 (3) (2017) 630–651.
- [3] Choi, S., Enhancing Thermal Conductivity of Fluids with Nanoparticles, ASME-Publications-Fed, 231 (1995), pp. 99-106.
- [4] K Koo, J., Kleinstreuer, C., A New Thermal Conductivity Model for Nanofluids, Journal of Nanoparticle Research, 6 (2004), 6, pp. 577-588.
- [5] Das, S. K., et al., Temperature Dependence of Thermal Conductivity Enhancement for Nanofluids, Journal of Heat Transfer, 125 (2003), 4, pp. 567-574.
- [6] M.A. Samad, M. Mansur-Rahman, Thermal radiation interaction with unsteady MHD flow past a vertical porous plate immersed in a porous medium, J. Nav. Architect. Mar. Eng. 3 (1) (2006) 7–14
- [7] U. Khan, B. Adnan Ullah, H. Abdul Wahab, I. Ullah, M.A. Almuqrin, I. Khan, Comparative thermal transport mechanism in Cu-H2O and Cu-Al2O3/H2O nanofluids: numerical investigation, Waves in Random and Complex Media (2022) 1–16.
- [8] V. Rajesh, A.J. Chamka, D. Bhanumathi, S. Vijaykumar, Radiation and chemical reaction effects on unsteady MHD free convection flow of a dissipative

- fluid past an infinite vertical plate with Newtonian heating, Comput. Therm. Sci.: Int. J. 5 (5) (2013).
- [9] Barmon, A., Hasanuzzaman, M., & Hasan, M. K. (2024). Radiative and Lorentz's effects on MHD free convective mass and heat transfer time-dependent nanofluid flow across vertical perforated plate. *Alexandria Engineering Journal*, 104, 266-278.
- [10] Hasanuzzaman, M., Azad, M. A. K., & Hossain, M. M. (2021). Effects of Dufour and thermal diffusion on unsteady MHD free convection and mass transfer flow through an infinite vertical permeable sheet. SN Applied Sciences, 3(12), 882.
- [11] Ahmad, S., Rohni, A. M., & Pop, I. (2011). Blasius and Sakiadis problems in nanofluids. *Acta Mechanica*, 218, 195-204.
- [12] Tiwari, R. K., & Das, M. K. (2007). Heat transfer augmentation in a two-sided lid-driven differentially heated square cavity utilizing nanofluids. *International Journal of heat and Mass transfer*, 50(9-10), 2002-2018.
- [13] Raptis, A. (1998). Flow of a micropolar fluid past a continuously moving plate by the presence of radiation.

- International Journal of Heat and Mass Transfer, 18(41), 2865-2866.
- [14] Raptis, A. (1999). Radiation and viscoelastic flow. International Communications in Heat and Mass Transfer, 26(6), 889-895.

## NOMENCLATURE

(u,v): velocity components,  $(ms^{-1})$ 

T: nanofluid temperature, **K** 

g: acceleration due to gravity,  $(ms^{-2})$ 

C: nanofluid concentration,  $(kg. m^{-3})$ 

 $k_T$ : thermal diffusion ratio,  $(m^2 s^{-1})$ 

T: temperature, K

 $D_{m_{nf}}$ : nanofluid mass diffusivity coefficient,( $m^2s^{-1}$ )

 $\mu_{\rm nf}$ : nanofluid dynamic viscosity, (*N*.  $sm^{-2}$ )

 $\rho_{\rm nf}$  nanofluid density,  $(kg. m^{-3})$ 

 $v_{\rm nf}$ : nanofluid kinematic viscosity,  $(sm^{-2})$ 

 $k_{nf}$ : nanofluid thermal conductivity,  $(\boldsymbol{W}\boldsymbol{m}^{-1}\boldsymbol{K}^{-1})$ 

 $\beta_{\rm nf}$ : volumetric expansion coefficient, ( $K^{-1}$ )

t : time (**S**)

 $(\rho c_p)_f$ : heat capacitance of base fluid,  $(J. Kg^{-1}K^{-1})$ 

φ : nanoparticle volume fraction